Graphene-AuNP enhanced Inkjet-printed Silver Nanoparticle Paper Electrodes for the Detection of Nickel(II)-dimethylglyoxime [Ni(dmgH$_2$)] complexes by Adsorptive Cathodic Stripping Voltammetry (AdCSV)

Keagan Pokpas*[1], Nazeem Jahed[1], Earl McDonald[2], Petrone Bezuidenhout[3], Suzanne Smith[3,4], Kevin Land[3,4], and Emmanuel Iwuoha[1]

[1] *SensorLab, Department of Chemistry, University of the Western Cape, Robert Sobukwe Road, Bellville, 7530, South Africa,*

[2] *Electron Microscope Unit, Physics Building, University of the Western Cape, Robert Sobukwe Road, Bellville, 7530, South Africa,*

[3] *Materials Science and Manufacturing, Council for Scientific and Industrial Research (CSIR), Meiring Naude Road, Brummeria, Pretoria 0001, South Africa.*

[4] *Department of Electrical, Electronic, and Computer Engineering, University of Pretoria, Hatfield 0028, South Africa*

Corresponding Author:
*Keagan Pokpas**

Email: kpokpas@uwc.ac.za
Tel: +27 21-959 4038

Email addresses and ORCID numbers:

KP:	kpokpas@uwc.ac.za	https://orcid.org/0000-0002-4856-0053
NJ:	njahed@uwc.ac.za	https://orcid.org/0000-0001-8327-1970
EM:	emcdonald@uwc.ac.za	
PB:	u11038757@tuks.co.za	https://orcid.org/0000-0001-7745-4068
SS:	suzanne.smith@up.ac.za	https://orcid.org/0000-0002-3688-1845
KL:	kevin.land@up.ac.za	https://orcid.org/0000-0002-8803-8809
EI:	eiwuoha@uwc.ac.za	https://orcid.org/0000-0001-6102-0433

Graphical Abstract:

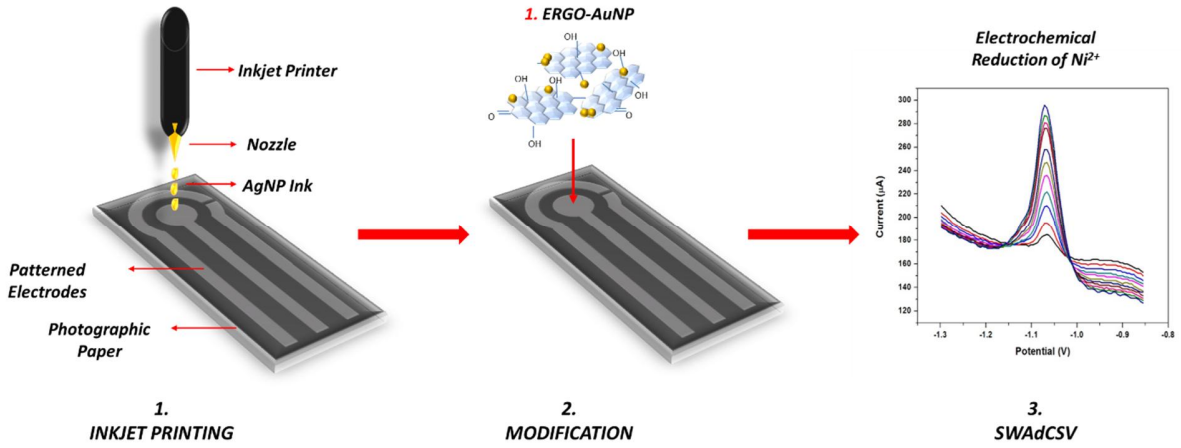

Abstract:

The development of low-cost, disposable electrode materials has been at the forefront of sensor technology in recent decades. Paper, offers possibilities for multi-functional, disposable and economically friendly sensing capabilities and has proved to be a suitable reagent storage and substrate material in paper-based analytical devices (PADs). In this work, we report a simple inkjet printing procedure on photographic paper for the fabrication of single analyte electrochemical sensors. A three-electrode system, consisting of a 3 mm diameter working electrode (WE), a counter electrode (CE) and a reference electrode (RE) were prepared by inkjet printing of silver conductive inks for comparison to common commercial screen printed electrode (SPE) brands. In a second step, carbon coating and modification of the working electrode surface with an electrochemically reduced graphene oxide, gold nanoparticle (ERGO-AuNP) film, to improve electrode sensitivity and selectivity was employed. Improved electron-transfer kinetics, increased active surface area and enhanced catalytic properties were achieved due to the ERGO-AuNP layer inclusion. Electrical and topographical characterization of the printed layers was performed in the fabrication process. Printing of Ag-NP ink showed good resistivity (1.8 – 6.3 Ω) on photographic paper. The prepared printed paper-based electrodes (PPE) offer a quantitative analysis of Ni(II), based on the accumulation of $Ni(dmgH)_2$ complexes at the modified electrode surface by square-wave adsorptive cathodic stripping voltammetry (SW-AdCSV). This study offers the first investigation on the feasibility of adsorptive electrochemical sensing methods at porous cellulose paper-based substrates. Instrumental parameters including deposition potential and deposition time were optimized for both electrochemical sensors. Improved sensitivities were achieved at the modified integrated electrodes over the

unmodified derivate with a limit of detection (LOD) of 32.19 μg L^{-1} achieved for the ERGO-AuNP-CC-Ag-PPE. This is well below the EPA and WHO standards of 0.1 mg L^{-1} or 0.1 ppm for Ni^{2+} in drinking water.

Keywords:

Adsorptive cathodic stripping voltammetry, dimethylglyoxime, graphene-gold nanocomposite, Nickel analysis, Printed paper-based electrochemical devices.

Highlights:

- Inkjet printing in conjunction with a screen-printing technique was employed towards the development of integrated three-electrode systems on paper substrates comparable to commercial screen-printed electrode designs.
- Simultaneous electrochemical reduction of graphene oxide decorated with gold nanoparticles, in conjunction with dimethylglyoxime complex was for the first time employed to enhance electrode sensitivity in paper-based analytical devices.
- The fabricated, modified paper-based sensors were for the first time successfully applied towards the adsorptive cathodic stripping voltammetric (AdCSV) detection of Ni^{2+} ions in water showcasing the possibility for adsorptive detection methods at porous substrates.
- Electrodes modified with ERGO-AuNP improved sensitivity and detection towards Ni^{2+}in adsorptive detection techniques over unmodified paper-based sensors by improving electron-transfer kinetics, increasing the active surface area and enhancing catalytic properties toward metal detection.
- Sensitive, accurate, disposable and cost-effective sensors based on paper substrates were developed with great potential in the field of electrochemical sensing and offered the first application of paper-based printed sensors for adsorptive stripping voltammetric detection.

1. Introduction

The ongoing demand for industrialization in modern society has led to a remarkable increase in environmental pollution of groundwater systems by heavy metal contaminants. This form of pollution poses particularly harmful effects on biological systems when inhaled and ingested. Heavy metals including lead, cadmium, copper, nickel, and

cobalt have been linked to a range of illnesses due to their toxic nature and ability to accumulate in biological organs [1,2]. Exposure to nickel, in particular, occurs through refineries, power stations, eating and drinking of contaminated foods, handling nickel-based coins and cigarette smoking [3] all of which remain prevalent in developing countries in particular. Nickel is often found in the body at extremely low levels, < 10 mg [4] and in the low μg L^{-1} concentration levels in water samples [5] but is able to bioaccumulate and pose toxic effects. While nickel poisoning often remains undiagnosed, illnesses including dermatitis, fibromyalgia, cancer, myocarditis, infertility, prostate conditions and allergic reactions have been linked to nickel toxicity [6]. Therefore, effective and reliable monitoring of exposure remains pivotal to environmental scientists and health practitioners alike.

Miniaturized and portable electrochemical sensing devices have gained significant traction with the rapid expansion of lab-on-a-chip technologies to alleviate the problems surrounding the expensive instrumentation and large sample volumes associated with spectroscopic methods. Paper-based electroanalytical devices (PEDs) have been explored by analytical chemists owing to their sensitivity, low sample volume (μL) and lack of need for unskilled labour. PEDs have made tremendous strides in recent times due to their ability to combine the advantageous properties of electrochemical sensing with paper substrates. Paper is inexpensive, easily modified, a good filter, biodegradable/disposable, porous and biocompatible, making it the ideal material for analytical applications. Electrochemical methods coupled with stripping voltammetric techniques relying on pre-concentration of the electrode surface have been demonstrated as a viable method for metal determination in on-site analysis. Here, simultaneous, sensitive, inexpensive and low-concentration detection is achieved. Although there is great potential for paper substrates as electrochemical sensor devices, improvements in fabrication, analysis techniques, sensitivity, and reproducibility are still required to meet the standards set by other known substrates.

A variety of fabrication methods have been studied to develop integrated electrode systems on flexible and paper substrates. Photolithography [7–11], sputtering [12–14], screen printing [15–19], inkjet printing [20–25], hand-drawing [26], among others have all been investigated to date. Drop-on-demand inkjet printing has proven to be a low-cost and time-saving alternative to commonly used photolithography [27] due to its ability to accurately pattern substrates by delivering low volume of material without the use of masks (template, stencils or resists to prevent liquid spreading) while avoiding contact with the substrate [28]. High conductivity, small particle sizes and features in the low micrometre range are among its most attractive attributes. PEDs relying on printed electrode systems are often employed to create integrated, lightweight and disposable sensing systems for limited use [29]. Recently an ever-

growing number of works have focused on drop-on-demand inkjet printing for the development of electrochemical sensors. Potentiometric ion [30], glucose [31], pH [32,33], dissolved oxygen [34], hydrogen peroxide [32] and ascorbic acid [35] detection, among others have been investigated to date. While metal analysis at PEDs have developed rapidly, their analysis at these inkjet-printed PEDs at present remains in their infancy stage. Combined stripping voltammetric techniques with printed paper electrodes have not yet been investigated to date.

Electrochemical stripping analysis has widely been established as a powerful alternative analytical tool over more costly molecular and spectroscopic techniques for the determination of pharmaceuticals, organic compounds, biological samples and metal ions, among others. Owing to the preconcentration of the electrode surface, stripping voltammetry offers ultra sensitivity, low detection limits, short analysis times and the possiblity for on-site analysis [36,37]. For a number of decades stripping voltammetry has gained a reputation as the go-to electrochemical technique for determination of a number of metal ions including lead, cadmium, mercury, silver, copper and nickel with anodic stripping voltammetry (ASV) being the most popular [38]. This technique, however, is limited to only a select number of metal species which can be electrolytically deposited on or form an amalgm or fused alloy with mercury or metal films such as bismuth, antimony and lead at the electrode surface. Adsorptive stripping voltammetry (AdSV), readily used for less electroactive metal ions reiles on the formation and non-electrolytic adsorption of sparingly soluble salts in the presence of a suitable chelating agent or ligand during the preconcentration step [39]. The method has shown tremendous application for detection of nickel, cobalt, thalium, galium, chromium, among others in water and food samples alike. At present, a number of electrode modification techniques are utilized to improve the sensitivity, selectivity, antifouling behavior and electron transfer kinetics of stripping voltammetric techniques. Of these, metallic modifications remain crucial in the analysis of metal ions and have been well documented. Metal electrodes [40–43], metallic films [44–47] and metal nanoparticles [48–50] have been extensively studied to improve the detection efficiency of the AdSV technique. To date, all work dedicated to the electrochemical sensing of metals at paper-based sensing devices have been limited to ASV approaches. No literature has been reported on the use of paper-based sensors in AdSV applications relying on non-electrolytic accumulation of the metal species at the paper surface.

The study of carbon nanomaterials to improve electrode sensitivity as a direct result of their enhanced electron transfer kinetics and the improved surface area-to-volume ratio has kept materials scientists fascinated for the last two decades [51,52]. Graphene, the 2D carbon nanomaterial along with its oxides (graphene oxide) and other carbon nanoparticles including carbon nanotubes, carbon black, onion-like carbon and carbon dots have all been incorporated into

electrochemical sensing applications [51–57]. In particular, the ability to improve paper-electrode sensitivity and selectivity through gold nanoparticle decorated graphenes has not been studied.

In this work, we report the design of a well-referenced paper-based three-electrode system to be used as PED for the first electrochemical adsorptive stripping analysis of metal ions in water samples. Here, drop-on-demand inkjet printing of silver nanoparticle-based inks in conjunction with gold nanoparticle decorated carbon nanomaterials (graphene) were employed for the development of highly conductive electrode systems on commercial photographic paper substrates. The modified fabricated printed paper-based electrochemical devices (PPEDs) along with dimethylglyoxime ($C_4H_8N_2O_2$) complexing agents were employed for the electrochemical detection of Ni^{2+} metal ions as the testing standard in water by adsorptive cathodic stripping voltammetry (AdCSV). The system is based on the accumulative non-electrolytic adsorption of metal-chelate complexes [$Ni(dmgH)_2$] at the surface of porous carbon nanomaterial modified inkjet-printed paper working electrodes in conjunction with an in-situ plated metallic film [58]. This study demonstrates the first report on the feasibility of adsorptive stripping voltammetric techniques in paper-based sensing which, to date, has not yet been investigated or thought possible.

2. Materials and Apparatus

2.1. Apparatus

Conventional, low-cost three-electrode electrochemical systems were fabricated by Inkjet-printing of silver nanoparticle conductive inks. A Fujifilm Dimatix DMP-3281 materials deposition printer was employed for all inkjet printing at the Council for Scientific and Industrial Research (CSIR), Pretoria, South Africa. All designs were created using eMachineShop free design software in conjunction with DesignCAD. Readily available Penguin photo paper, premium hi gloss (A4, 21.0 x 29.7 cm) was obtained from the CSIR. Greyscale tests were performed using an image analysis software: Image J. Laser profilometry was performed using a Zeiss LSM5 Pascal confocal laser scanning microscope.

All electrochemical voltammetric experiments were performed with a Metrohm Autolab PGSTAT101 instrument, in combination with the Nova 1.11 Software and controlled by a personal computer. All electrochemical experiments were performed in one compartment 20 mL voltammetric cells at room temperature unless stated otherwise. A conventional hotplate and vacuum oven, obtained from Labotec were utilized for wax melting and sintering of conductive inks respectively.

2.2. Chemicals and Reagents

All chemicals used in the study were of analytical reagent grade. Ultra-pure distilled water (Millipore) was used to prepare all solutions. Harima NPS-JL-nano-silver ink, for low-temperature curing (Harima Chemicals Group) and carbon conductive paste for screen printing (Gwent Group), was used without modification. Nafion perfluorinated resin solution 5 wt. % in lower aliphatic alcohols and water, 2,3-Butanedione-dioxime (Dimethylglyoxime) and Nickel(II), Cobalt(II), Mercury(III) and Gold(III) standard stock solutions (1 000 mg L^{-1}, atomic absorption standard solution) and all other metal standards were obtained from Sigma-Aldrich and diluted as required. Natural graphite powder (microcrystal grade, 99.9995%, Metal base) UCP1-M grade, Ultra "F" purity and carbon black was purchased from Alfa Aesar. Ammonia/Ammonium Chloride (NH_3/NH_4Cl) buffer solution (0.1 M, pH 9.3), prepared by mixing appropriate quantities of ammonia (NH_3) and ammonium chloride (NH_4Cl) was used as supporting electrolyte for all studies. A Metrohm 827 pH lab pH meter was calibrated using pH 4 and 7 calibration buffer solutions and then used to verify the pH of the prepared NH_3/NH_4Cl buffer solution.

3. Experimental Methods

3.1. Design and Fabrication of Carbon-Coated AgNP Inkjet-Printed Electrodes

A piezoelectric materials printer was used to carry out all inkjet printing. The printing of features was performed at 30 ^oC using a 10 pL drop-volume DMCLCP-11610 Dimatix materials cartridge on Penguin photographic paper substrates. Harima NPS-JL-nano-silver ink was investigated under optimized printing parameters. Figure 1A and 1B show patterned three-electrode systems, with small and large contacts respectively designed by computer assisted design software for screen-printed electrode cable or crocodile clamp use. Typically, nano-silver working (3 mm diameter), counter and reference electrodes, electrical tracks, and electrical contacts were developed and are illustrated along with appropriate dimensions. The electrode design was chosen based on commercial screen printed electrodes purchased from Metrohm Dropsens, Spain. A schematic illustration of the PPED fabrication process is shown in Figure 1C. Carbon screen-printing of the CE and WE follows inkjet printing of desired silver electrode patterns on low-cost hydrophobic paper substrates. Post printing sintering at 160 ^oC was conducted to evaporate carrier solvent and additional non-conductive binding materials present in the ink to allow for optimal conductivity due to contact between the metallic materials. Figure 1D is an image of a single sheet of printed electrode arrays. Reproducible electrode designs were created by the developed printing procedure. Carbon ink was diluted to appropriate viscosity

and screen-printed onto working and counter electrodes. The coated electrodes were allowed to dry in a vacuum oven at 85 ^{o}C for 1 hr. Vinyl coatings prevent solution flow to electrical contacts. Figure 1E shows images of the manufactured paper-based electrodes before and after carbon screen printing.

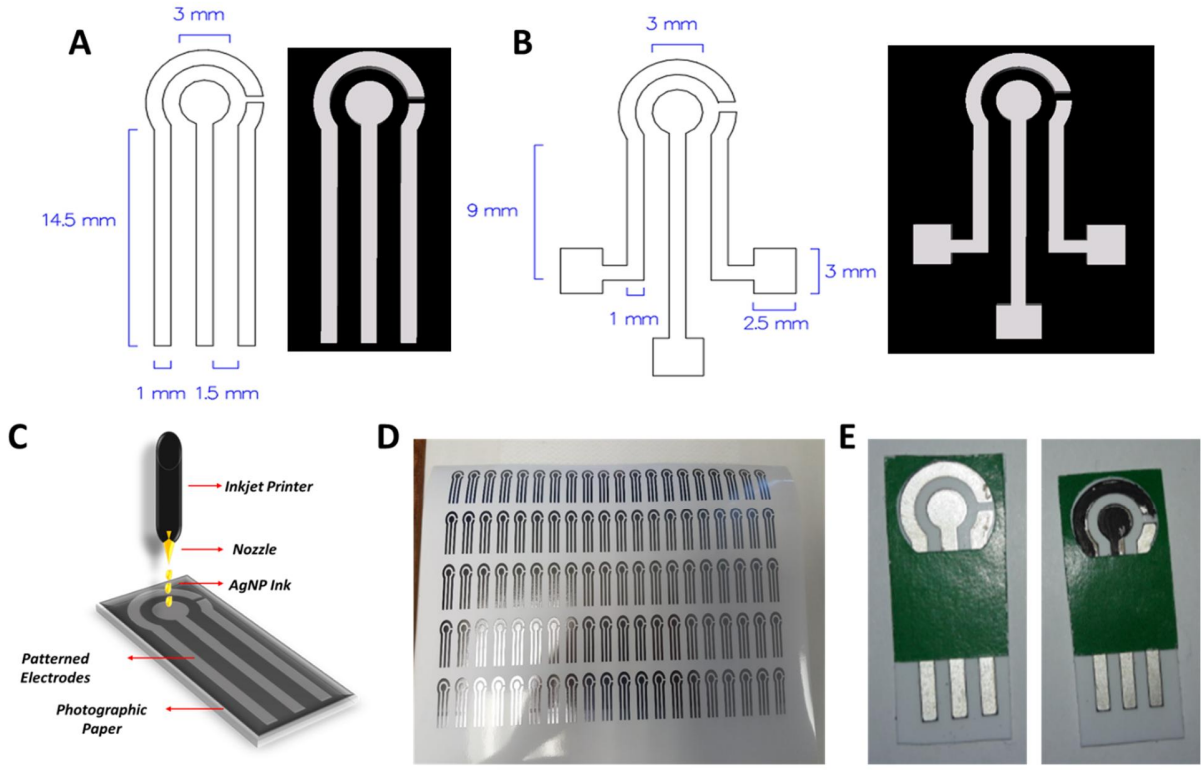

Figure 1: **A**. A schematic illustration of inkjet-printed three-electrode system design with small contacts. **B**. Design of large contacts for crocodile clamp use. **C**. An illustration of the PPEC fabrication process. **D**. An array of printed AgNP electrodes on photographic paper. **E.** Inkjet-printed paper electrode systems before and after carbon coating.

3.2. Preparation of Electrochemically Reduced Graphene Oxide, Gold Nanoparticle, Carbon-coated Silver Printed Paper-based Electrodes (ERGO-AuNP-CC-Ag-PPE)

A modified Hummer's method [59] was employed for the synthesis of graphene oxide (GO) [37] by mixing appropriate quantities of graphite powder, sodium nitrate and potassium permanganate in sulfuric acid. The prepared GO (5 mg) was exfoliated in 10 mL 0.1 M acetate buffer solution (pH 4.6) with 15 ppm Au solutions by ultra-sonication for 1.0 hour, before use. Prepared carbon coated silver printed paper-based electrodes (CC-Ag-PPE) were immersed in 10 mL of GO-Au solutions (0.5 mg mL^{-1} GO and 15 ppm Au) and the cyclic voltammetric reduction was

performed under hydrodynamic conditions between -1.4 and 0.5 V [37]. CV parameters including accumulation potential (E_{acc}), accumulation time (t_{acc}), amplitude (*Ampl.*), frequency (f) and voltage step (E_{step}) were: E_{acc} = -1.4 V, t_{acc} = 120 s, f = 50 Hz, *Ampl.* = 40 mV and E_{step} = 4 mV. ERGO-AuNP-CC-Ag-PPEs were dried at room temperature for 30 min before use.

3.3. Procedure for the SW-AdCSV analysis of Ni^{2+}

The N-DMG-CB-Ag-PPE and ERGO-AuNP-CC-Ag-PPE were immersed in a 20 mL electrochemical cell containing 10 mL of (a) appropriate concentrations of Ni^{2+} and (b) appropriate concentrations of Ni^{2+} in the presence of 2 mM DMG and 10 mg L^{-1} Hg^{3+} respectively. *In-situ* simultaneous accumulation of $Ni(dmgH)_2$ onto the working electrode was performed at E_{acc} = - 0.7 V and t_{acc} = 120 s. Ammonia (NH_3/NH_4Cl) buffer (0.1 M, pH 9.4) was used as a supporting electrolyte. The SWV parameters were as follows: E_{begin} = -0.7 V, E_{end} = -1.35 V, f = 5 Hz and *Ampl.* = 10 mV.

4. Results and Discussion

4.1. Morphological and Topological Studies of the Inkjet Printed Paper-based Features

Surface morphology, topography and printed dimensions of the as printed AgNP inks on paper-based substrates were studied prior to use. High-resolution scanning electron microscope (HRSEM) imaging of the inkjet-printed AgNP working electrode, WE on photographic paper substrates, at 50X magnification is shown in Figure 2A. Well-defined, smooth features with distinct edges and little-to-no spreading or spurious droplets are shown. A uniform film with clear boundary was patterned on the surface of the hydrophobic paper substrate. The metallic AgNP appears as a clear bright region on the microscope image due to a large number of scattered electrons associated with its metallic structure. Small defect areas and oxidation of the AgNP film is observed. The energy dispersive X-ray spectra (EDS), Figure 2B confirms the inclusion of Ag at 3.1 keV while the carbon peak is attributed to carbon-coating during the HRSEM sample preparation procedure. An array of dog-bone structures with varying line thicknesses (Figure 2C), between 0.1 – 1.5 mm was used to study the topographical nature of the printed designs further. Laser microscope images of precise printed features after thermal curing are shown in Figure 2D below and correlate to the HRSEM results (Figure 2A). The hydrophobic resin surface reduces ink spreading creating more precise droplet formation resulting in sharp edges at printed boundaries with only a few defects in the printed surface. Some residual ink spatter can be observed at the right edge which may be attributed to non-spherical droplet formation in machining. Striations

in the printed pattern occur as a result of printing progression. Laser profilometry was further used to probe laser micrograph cross-sections of the dog-bone structure arrays printed on photographic paper. Figure 2E shows a typical laser micrograph of the 0.5 mm AgNP inkjet-printed feature. Relatively uniform film thickness with clearly defined patterns and excellent resolution is observed. No absorption of the Ag-ink was seen by the photographic paper. Remarkable contrast is shown between the hydrophobic resin and Ag-film. Topographical analysis of the electronic tracks was used to examine the thickness and width of the printed 0.5 mm design. A single printing pass was found to have a roughness of 0.52 µm, a thickness of 25.7 µm and a line width of 0.58 mm. Similar results were reported in the work by Joubert et al. [60].

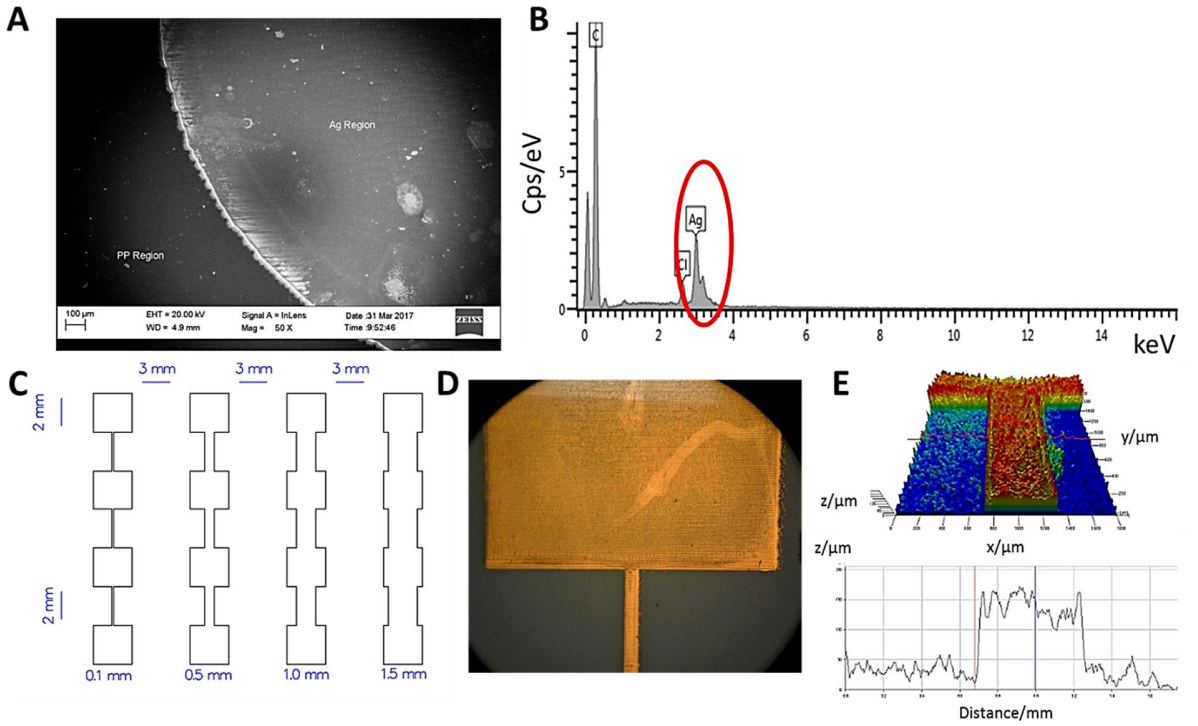

Figure 2: **A**. An HRSEM image of the Inkjet printed Ag WE on photographic paper substrates and **B**. An EDS spectra of the AgNP-film. **C**. A schematic illustration of the designed dog-bone array. **D**. Laser microscope image of the inkjet printed 0.1 mm AgNP track on photographic paper. **E**. Laser micrograph and corresponding laser profilometry of the 0.5 mm cross-section.

4.2. Electrical Characterization of the Printed Ink

The effect of the sintering/curing temperature of silver inks on the resistance of single layer printed tracks was investigated between 25 – 200 ºC for penguin photographic paper and the results are recorded in Figure 3A. An overall decrease in measured resistance was observed with increasing line width for all temperatures measured. Improved resistance values at temperatures greater than 25 ºC showed the improved removal of solvent and binder materials. Temperatures of 120 and 160 ºC respectively proved to be ideal for thermal sintering with similar measured resistance in the 1.8 – 6.3 Ω range. In contrast, a considerable increase in measured resistance is noted for sintering temperatures of 200 ºC as warping and burning of the hydrophobic resin took place (Figure 3B). Further, printed features with dimensions greater than 0.1 mm demonstrated low resistance values by introducing adequate amounts of conductive particles.

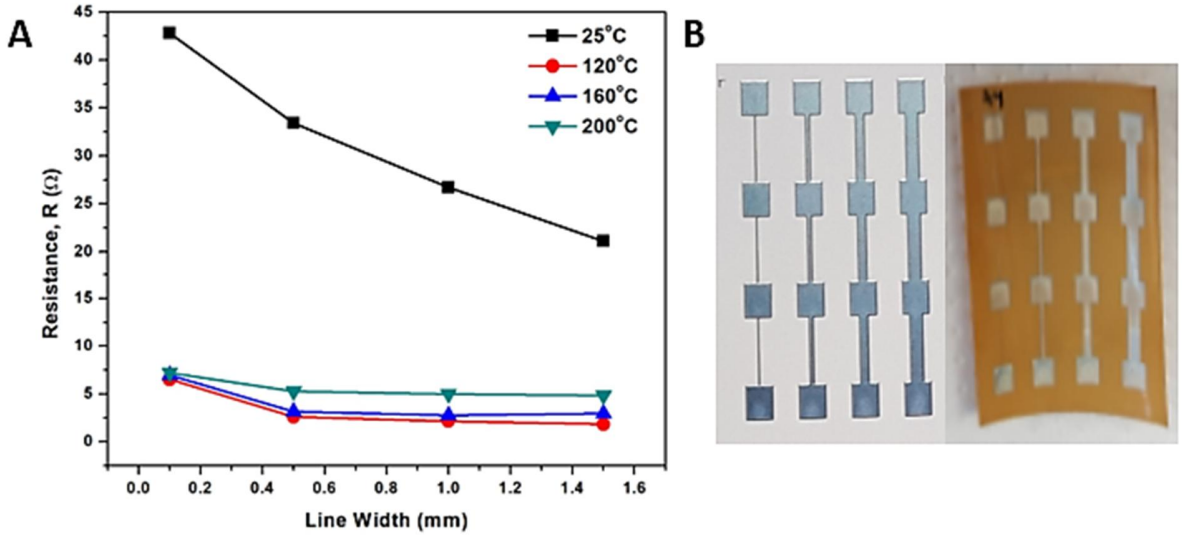

Figure 3: **A**. Measured resistance of Ag-ink tracks as a function of room and sintering temperature on photography paper. **B**. Dog-bone structures before and after curing at 200ºC for 1 hour.

Table 1 is a summary of the average electrical parameters (resistance, resistivity, conductivity and sheet resistance) recorded for 5 replications as a function of line width (0.1 – 1.5 mm). A decrease in average resistance was measured with increasing line width due an increase in the cross-sectional area of the printed dimensions. The thicker printed features have greater amounts and tighter packing of the conductive AgNPs present facilitating electron transport and

decreasing the resistance. Printed track features of 1.5 mm showed the best resistance. Resistivity (ρ) further relates the average resistance to the printed track dimensions:

$$\rho = R\left(\frac{wt}{l}\right) \qquad (1)$$

Where, R is the measured resistance for a track width, w, with thickness, t and length, *l* for the printed dimension. A more comprehensive analysis of the AgNP ink is provided by comparing sheet resistance (R_{sh}) according to Equation 2:

$$R_{sh} = \left(\frac{\rho}{t}\right) \times \left(\frac{w}{l}\right) (2)$$

Table 1: A summary of the recorded electrical parameters; resistance, resistivity, conductivity and sheet resistance for the Ag ink on photography paper after curing at 120°C for 1 hour.

Electrical Parameter	Line width (mm)			
	0.1	0.5	1	1.5
Average Resistance (**Ω**)	6.530	2.610	2.140	1.820
Resistivity (**Ω** mm)	0.001	0.001	0.002	0.002
Conductivity (1/**Ω**)	9.188	4.598	2.804	2.198
Sheet Resistance (**Ω**/sq.)	0.109	0.218	0.357	0.455

4.3. Preliminary Electrochemical Testing of Ag-printed Electrodes

Cyclic voltammograms of 5 mM $Fe(CN)_6^{3-/4-}$ solution in 0.1 M KCl recorded at (a) bare and (b) carbon-coated Ag-PPPE (printed photographic paper electrodes) is shown in Figure 4A. Large, broad peaks with a current overload at negative potentials and oxidation and discoloration of the working electrode surface (Figure 4A, inset) is observed for the uncoated Ag-PPPEs due to a high charging or capacitive current. Conversely, carbon-coating of the working and reference electrode surfaces by screen-printing showed a considerable decrease in IR difference and capacitive current and a discernable redox couple for the reversible $Fe(CN)_6^{3-/4-}$ solution was shown. The electrochemical impedance spectroscopy (EIS) was performed in a 5 mM $Fe(CN)_6^{3-/4-}$ solution between 0.1 – 10 000 Hz. Figure 4B shows the Nyquist plots of the Ag-printed paper electrode and the carbon-coated Ag-printed paper electrode. The inset is a magnified plot of the recorded impedance between 50 – 85 Ω. The EIS spectra show extremely conductive electrodes with very fast electron-transfer. The R_{ct}, represented by the semi-circle region of the Nyquist plot is 4.8 and 16.1 Ω

respectively. This confirms the results from the CV analysis in Figure 4A where the carbon coating decreases the electrode conductivity and reduces oxidation of the Ag-WE.

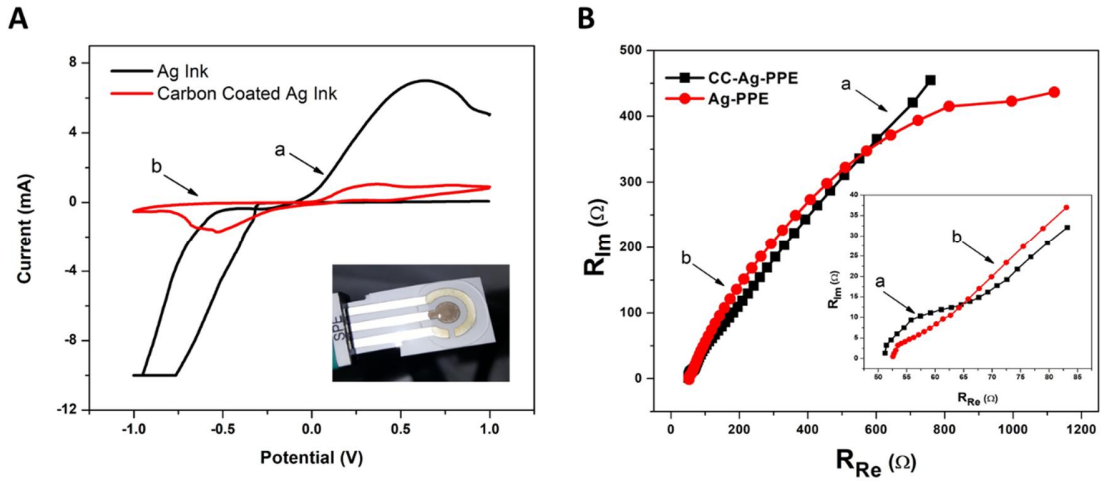

Figure 4: **A**. Cyclic voltammograms Electrochemical Characterisation (Inset: Oxidized Ag-PPPE) and **B**. Nyquist EIS plot (Inset: Enhanced 50-85 Ω R_{Re}) of (a) Ag-printed photo-paper electrode and (b) CC-Ag-printed photo-paper electrode in 5 mM $Fe(CN)_6^{3-/4-}$ at scan rate of 10-100 mV s^{-1} in supporting electrolyte (0.1 M KCl).

4.4. Electrochemically Reduced Graphene Oxide – Gold Nanoparticle, Silver Printed Paper-based Electrodes (ERGO-AuNP-CC-Ag-PPE)

4.4.1. Electrochemical reduction of Graphene oxide and gold nanoparticles

Here, a direct electrochemical cyclic voltammetric reduction approach, following a constant potential reduction at – 1.4 V for 30 s was adopted for the preparation of electrochemically reduced graphene oxide, gold nanoparticle (ERGO-AuNP) composite paper-based electrodes. The control attributed to the deposition of graphene sheets on the electrode surface was crucial to the development of the sensor. Figure 5A, depicts the repetitive (5 cycles) cyclic voltammograms of (a) 0.5 mg mL^{-1} GO suspensions and (b) simultaneous reduction of 0.5 mg mL^{-1} GO colloidal suspensions with 15 ppm Au^{3+} onto carbon-coated silver nanoparticle printed photographic paper electrodes (CC-AgNP-PPPE) between – 1.5 and 0.5 V. Two anodic (A and B) and three cathodic (A_1, B_1, and C_1) peaks are demonstrated in cyclic voltammograms of both the ERGO and ERGO-AuNP CC-Ag-PPEs, respectively. In the absence of gold salt, the redox couple with E_{pa} = 0.136 V and E_{pc} = 0.117 V, denoted by A and A_1, respectively appear with relatively low peak currents and are attributed to the reversible oxidation and reduction of the AgNP WE surface

as shown in the CV of the ERGO-CC-Ag-PPEs. A reduction in their associated peak currents is observed with an increasing number of scans as graphene sheets are deposited at the electrode surface preventing the oxidation and reduction of the substrate electrode surface. The redox couple B and B_1 at E_{pa} = - 0.49 V and E_{pc} = - 0.72 V confirms the deposition of graphene sheets at the electrode surface due to the reduction of GO in direct contact with the electrode surface. Electrostatic adsorption binds the formed graphene sheets to the electrode surface and a persistent increase in redox peak current with increasing successive potential cycles is further noted. The electrochemical reduction of graphene oxide could be attributed to the reduction of the functional groups including – OH and – COOH on the graphene oxide surface at negative potentials. A third reduction peak shown at C_1 (- 0.427 V) as a result of the reduction of oxygen moieties at the electrode surface is seen. Similar results were obtained in the work by Wu *et al.* [61]. Gold nanoparticles formed within and on top of the deposited graphene sheets in the presence of 15 ppm Au^{3+} and facilitate the desired electrochemical reduction reaction. The inclusion of the produced AuNPs further improved the peak currents of both cathodic and anodic peaks due to improved conductivity and active surface area to volume ratio of the ERGO-AuNP-CC-Ag-PPE surface.

Comparative cyclic voltammograms recorded at the (a) CC-Ag-PPE, (b) ERGO-CC-Ag-PPE and (c) ERGO-AuNP-CC-Ag-PPE in acetate buffer solution (0.1 M, pH 4.6) are shown in Figure 5B. Carbon-coated Ag-PPEs show characteristic voltammograms in the recorded potential window between – 1.5 and 0.3 V. A single oxidation and two reduction peaks are observed between 0.1 and 0.25 V attributed to the redox processes of the CC-AgNP working electrode surface as expected. An increase in peak current, as well as an increase in capacitive current, is seen upon the formation of the graphene film at the electrode surface. Improved electron-transfer kinetics and an increase in the effective surface area are demonstrated for the ERGO-Ag-PPE. A dramatic increase in background and AgNP redox peak is shown for incorporation of AuNPs within the reduced graphene oxide sheets as previously discussed. The gold nanoparticles further improved the electron transfer due to its highly conductive nature. The nanocomposite material can, therefore, be used as an effective means of improving electrode sensitivity.

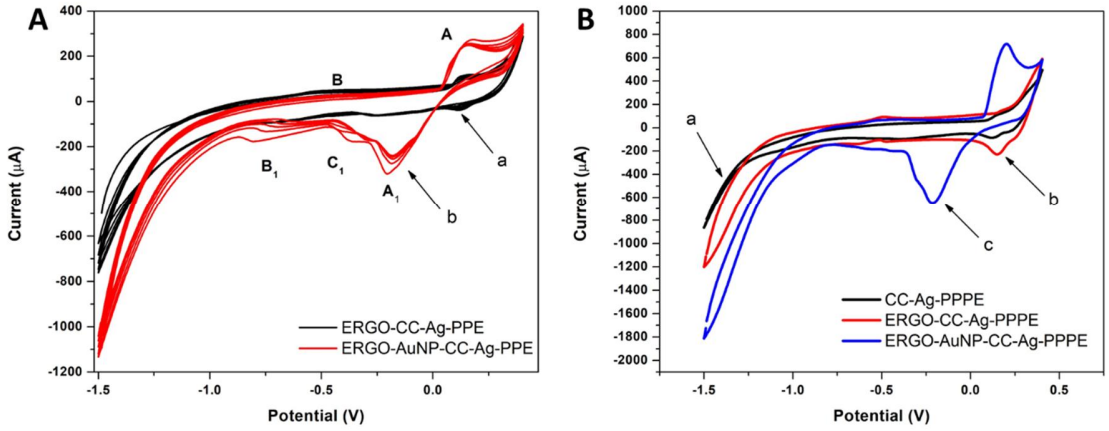

Figure 5: Cyclic voltammograms depicting **A.** the electrochemical reduction of 0.5 mg mL^{-1} GO and 15 mg L^{-1} Au^{3+} in acetate buffer solution (0.1 M, pH 4.6) at the CC-Ag-PPE and **B.** the (a) CC-Ag-PPE, (b) ERGO-CC-Ag-PPE and (c) ERGO-AuNP-CC-Ag-PPE in acetate buffer solution (0.1 M, pH 4.6), under the following instrumental parameters: scan rate (10 mV s^{-1}), deposition time (120 s); frequency (50 Hz); amplitude (0.04 V) and voltage step (0.004 V).

4.4.2. Electrochemical stripping performance of ERGO-AuNP-CC-Ag-PPE towards the Ni^{2+} detection

The electrochemical performance of the graphene and gold nanoparticle modified electrodes were investigated towards the detection of [Ni($dmgH_2$)] complexes by adsorptive cathodic stripping voltammetry. Figure 6A, depicts the recorded square-wave voltammograms (SWV) of 300 μg L^{-1} Ni^{2+} in the presence of 2 mM DMG and 10 mg L^{-1} Hg^{3+} at CC-Ag-PPPE, ERGO-CC-Ag-PPPE (5 – 30 cycles) and ERGO-AuNP-CC-Ag-PPPE (30 cycles). Stripping peak responses attributed to the reduction of [Ni($dmgH_2$)] complexes were observed between – 1.0 and – 1.2 V for all modified paper-based sensors. An increase in stripping peak current with the increasing number of graphene deposition cycles is observed in Figure 6B due to the favorable enhancement of electron transfer kinetics and improved electroactive surface area associated with graphene use. The ERGO-CC-Ag-PPPE with 30 deposition cycles was chosen for all further experiments to limit the formation of multilayer graphene sheets which inhibits the transfer of electrons responsible for the reduction of metal cations. A 400 % increase in stripping peak current when compared to the CC-Ag-PPPE. Simultaneous electrochemical deposition of ERGO and AuNPs onto the CC-Ag-PPPE surface

further improved the peak current response towards Ni^{2+} detection by 25 %. This outcome is in agreement with the hypothesised capabilities of metallic AuNPs to further improve electron transfer at the electrode surface.

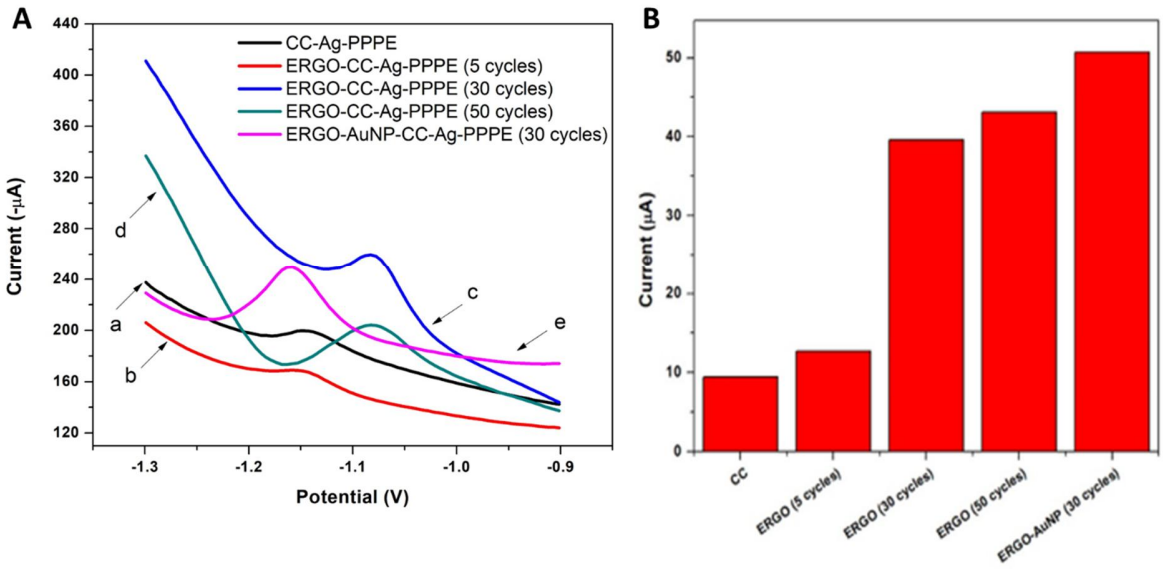

Figure 6: **A**. SW-AdCSVs and **B**. a comparison of 300 µg L^{-1} Ni^{2+} in the presence of 2 mM DMG and 10 mg L^{-1} Hg^{3+} at (a) CC-Ag-PPPE, (b) ERGO-CC-Ag-PPPE (5 cycles), (c) ERGO-CC-Ag-PPPE (30 cycles), (d) ERGO-CC-Ag-PPPE (50 cycles) and (e) ERGO-AuNP-CC-Ag-PPPE (30 cycles). Supporting electrolyte: 0.1 M NH_3/NH_4Cl buffer (pH 9.4). SWV instrumental parameters: E_{acc} = -0.7 V, t_{acc} = 120 s, f = 5 Hz and $Ampl$ = 10 mV.

4.4.3. Morphological Characterization of ERGO-AuNP-CC-Ag-PPPE

High resolution scanning electron microscopy (HRSEM) was utilized to probe the surface morphological changes of the photographic paper along the fabrication routes of the ERGO-AuNP-CC-Ag-PPPE. Figure 7, shows the HRSEM images of (a) inkjet-printed AgNP, (b) CC-AgNP, (c) ERGO-CC-AgNP and (d) AuNP-ERGO-CC-AgNP working electrodes on photographic paper at 5 kX magnification. The HRSEM image of patterned AgNP features on photographic paper by inkjet printing is shown in Figure 7A. A smooth, uniform film is observed on the photo-paper substrate. Relative, spherical particles are observed with no defects in the surface morphology. Figure 7B shows flake-like features deposited on the surface of the printed AgNP film. A rough, non-uniform topography is demonstrated. This is attributed to the homemade screen printing technique. Upon electrochemical reduction of 0.5 mg mL^{-1} suspensions of GO in 0.1 M acetate buffer solution (pH 4.6) for 5 cycles, wavy, few-layer sheets of graphene are

deposited on the carbon electrode surface (Figure 7C). The ERGO sheets are decorated across the electrode surface and resemble graphene sheets. Reduced graphene oxide is bound to the electrode surface by electrostatic attraction. The electrochemical reduction process was repeated in the presence of 15 ppm Au^{3+} and the formed ERGO-AuNP-CC-Ag-PPPE is shown in Figure 7D. Graphene sheets are deposited on the electrode surface and decorated with AuNPs trapped between graphene sheets.

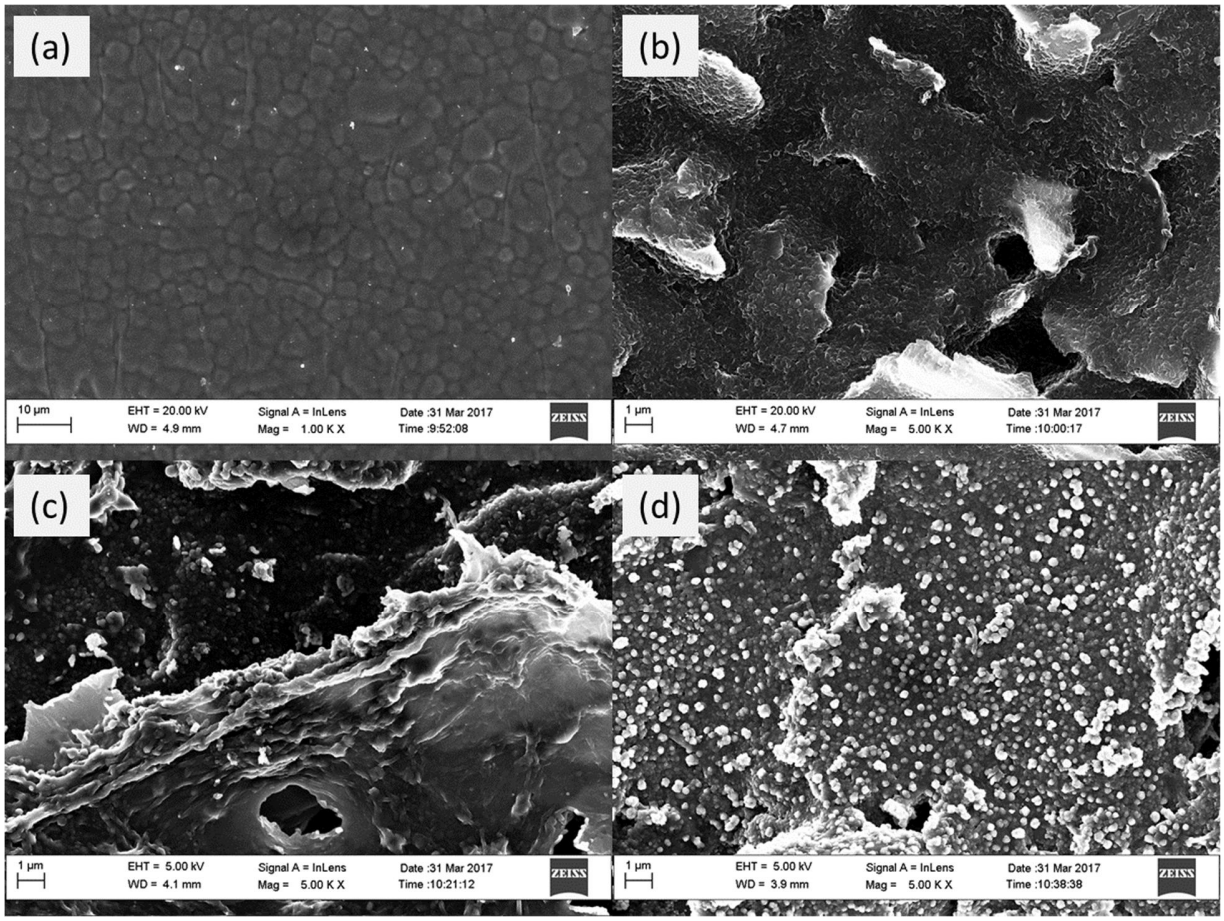

Figure 7: High resolution scanning electron microscope (HRSEM) images of (a) inkjet-printed AgNP, (b) CC-AgNP, (c) ERGO-CC-AgNP and (d) AuNP-ERGO-CC-AgNP working electrodes on photographic paper at 5 kX magnification.

4.4.4. Analytical performance of ERGO-AuNP-CC-Ag-PPPE

A 10-electron transfer reduction process governs the electrochemical detection of Ni^{2+} cations in the presence of DMG ligands and a metallic Hg-film at the ERGO-AuNP-CC-Ag-PPE. Here, the reduction of adsorbed $[Ni(dmgH)_2]$

complexes into Ni^0 and 2,3-bishydroxylaminebutane (DHAB) during a cathodic sweep results in a produced measurable current. The overall reduction is summarized in Equation 1 below, according to previous studies [62,63].

$$[Ni(dmgH)_2]_{ads}Hg + 10\,e^- + 10\,H^+ \rightarrow Ni(Hg) + 2\,DHAB \quad (1)$$

The ERGO-AuNP-CC-Ag-PPE acts as the working electrode for the determination of Nickel but does not participate in its overall electrochemical determination mechanism.

Figure 8, illustrates the dependence of adsorptive stripping voltammetric (AdSV) peak current response on the incorporation of chelating agent and metallic films at the electrode surface. Square-wave voltammetric responses of 300 µg L^{-1} Ni^{2+} recorded at the ERGO-AuNP-CC-Ag-PPPE in the presence of (a) 0.1 M NH_3/NH_4Cl buffer, (b) 2 mM DMG, (c) 10 mg L^{-1} Hg^{3+} and (d) 2 mM DMG and 10 mg L^{-1} Hg^{3+} under optimized instrumental parameters are shown. The absence of reduction peaks for buffer and Hg film electrodes, highlight the low sensitivity reduction of Ni^{2+} and its low-solubility in electroplated Hg-films. The inclusion of dimethylglyoxime as a chelating agent allows for soluble metal-ligand complex formation and its subsequent adsorption at the mercury coated electrode surface. A single, reversible, well-defined cathodic peak can be seen at – 1.15 V attributed to the reduction of the [Ni($dmgH_2$)] complex. Further, accumulation of the [Ni($dmgH_2$)] complex at an electroplated Hg-film, results in a two-fold increase in the electrolytic Ni^{2+} stripping peak current. The optimum Hg-ion and DMG complexing agent concentrations were studied and found to be 10 mg L^{-1} and 2 mM, respectively.

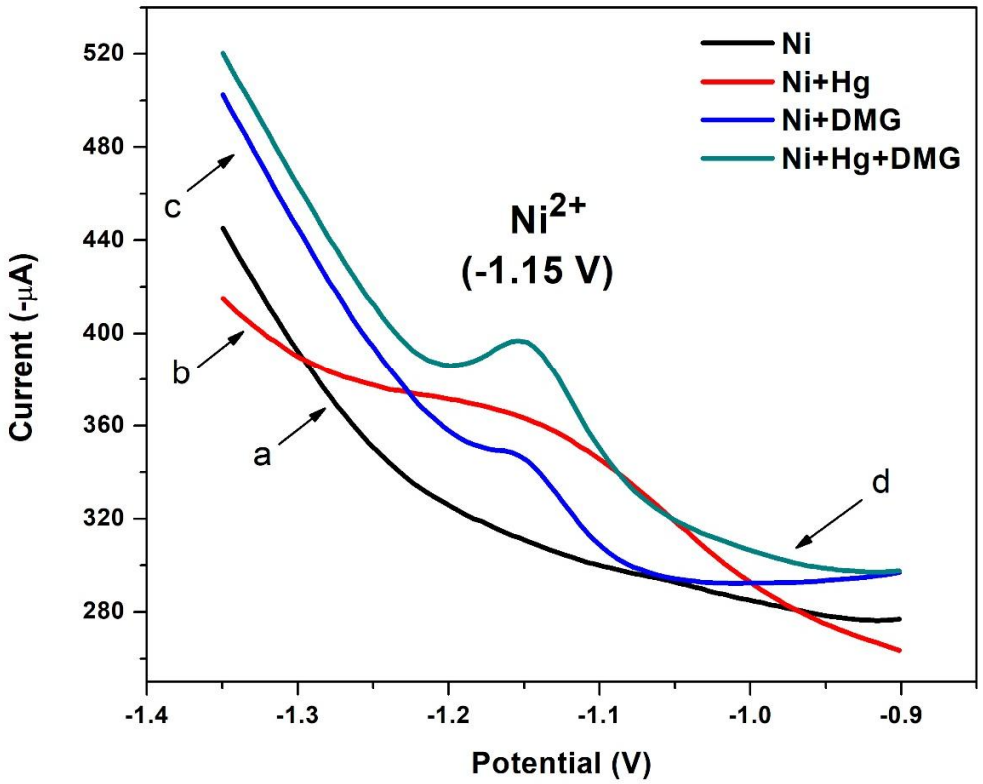

Figure 8: SW-AdCSVs of 300 µg L^{-1} Ni^{2+} at the ERGO-AuNP-CC-Ag-PPPE in the presence of (a) 0.1 M NH_3/NH_4Cl buffer, (b) 10 mg L^{-1} Hg^{3+}, (c) 2 mM DMG and (d) 2 mM DMG and 10 mg L^{-1} Hg^{3+}. Supporting electrolyte: 0.1 M NH_3/NH_4Cl buffer (pH 9.4). SWV instrumental parameters: E_{acc} = -0.7 V, t_{acc} = 120 s, f = 5 Hz and $Ampl$ = 10 mV.

4.5. Analytical Studies at the ERGO-AuNP-CC-Ag-PPPE

The analytical performances of the ERGO-AuNP-CC-Ag-PPPE was evaluated for Ni^{2+} detection in 0.1 M NH_3/NH_4Cl buffer solution (pH 9.4) under optimum conditions as follows: E_{acc} = - 0.7 V, t_{acc} = 120 s, E_{begin} = -0.7 V, E_{end} = -1.35 V, f = 5 Hz and *Ampl.* = 10 mV. The recorded SW-AdCSVs and corresponding calibration plot are shown in Figures 9 a and b, respectively. The performances of the sensors were investigated in the 50-500 µg L^{-1} [Ni^{2+}] range. A constant linear increase (R^2 = 0.996) in stripping peak current is observed with increasing Ni^{2+} concentration for the ERGO-AuNP-CC-Ag-PPPE over the entire studied concentration range (50-500 µg L^{-1}), with no significant shift in stripping

peak potential. Here, a higher concentration of Ni^{2+} ions are available for complexation with excess DMG to produce an increase in [Ni(dmgH_2)] complex formation and its subsequent adsorption at the electrode surface. A sensitivity of 1.38 x 10^{-7} µA L $µg^{-1}$ was achieved. Electrode saturation occurs at concentrations greater than 350 µg L^{-1} hindering the flow of the produced current and a deviation from linear calibration is observed. Figure 9B shows the recorded calibration plot. As predicted, due to the presence of the electroplated Hg-film the ERGO-AuNP-CC-Ag-PPE exhibited improved sensitivity (10 times) over the metal free version. Further, it could be surmised that improved electroactive surface area is achieved due to the incorporation of graphene at the electrode surface. The developed modified sensor showed accurate detection of Ni^{2+} over the concentration range investigated. The ERGO-AuNP-CC-Ag-PPE showed a significantly wide linear range as a direct result of its improved sensitivity towards metal cations.

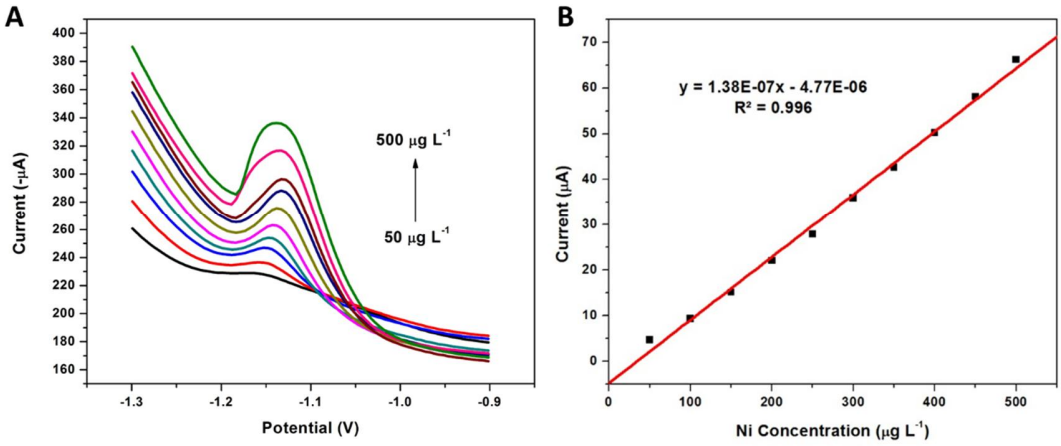

Figure 9: SWASV and corresponding calibration plot of individual analysis of Ni^{2+} obtained at the ERGO-AuNP-CC-Ag-PPE over 50 – 500 µg L^{-1} range. Supporting electrolyte (0.1 NH_3/NH_4Cl Buffer, pH 9.4), deposition time (90 s), deposition potential (- 0.7 V), rotation speed (1000 rpm), frequency (5 Hz), amplitude (0.01 V).

The detection limit (LOD) of the Ni^{2+} sensors were determined according to Equation 3:

$$D.L. = \frac{3\sigma}{slope} \qquad (3)$$

Where, D.L.; is the detection limit

3σ; is three times the standard deviation of the blanks

slope; is the gradient (slope) of the calibration curve

The standard deviation of the blanks was determined from 5 replications of the ERGO-AuNP-CC-Ag-PPPE in 0.1 M NH_3/NH_4Cl Buffer (pH 9.4). Calculated standard deviations were larger than hoped for due to an increase in background current with consecutive runs as previously stated due to charge build up at the electrode surface. Determined limits of detection and quantification were found to be 32.19 µg L^{-1} and 96.57 µg L^{-1} respectively at an analysis time of 120 s. The calibration and detection results are summarized in Table 2.

Table 2: A summary of recorded analytical data for the ERGO-AuNP-CC-Ag-PPE over the 50 – 500 µg L^{-1} range.

Analytical Parameter	*ERGO-AuNP-CC-Ag-PPE*
Sensitivity (µA L μg^{-1})	1.38×10^{-7}
Correlation Coefficient (R^2)	0.996
Detection Limits (µg L^{-1})	32.19 ± 9.61
Limit of Quantification (µg L^{-1})	98.57± 26.2

The observed limits of detection recorded at the ERGO-AuNP-CC-Ag-PPE are shown in Table 3, along with a summary of previously reported sensors for the detection of Ni^{2+} in test samples by AdSV. To date, no other studies have reported on the use of paper-based electrodes in adsorptive stripping voltammetric detection of metal ions and nickel, in particular. The recorded LODs are, therefore, compared to existing studies performed at solid carbon electrodes including; glassy carbon, screen-printed and carbon paste electrodes, to name a few. As predicted, the low LODs show that conventional solid electrodes provided the best sensitivity towards nickel detection due to the non-porous electrode surfaces better facilitating adsorption of the formed $Ni(dmgH)_2$ complexes. This is in agreement with the hypothesised findings where work is still required to improve the sensitivity of paper-based sensors due to the higher conductivity of the solid electrode materials over the porous cellulose alternatives [64,65]. Ko et al. further reported that traditional physical adsorption processes are limited in paper and textile substrates due to their large surface roughness and porosity [66]. The work on paper-based electrochemical cells in conjunction with screen-printed carbon electrodes, reported by our research group in 2017 further showcased that solid electrodes used in combination with paper-based cells also decreased the sensitivity over existing studies but demonstrated the feasibility of the use of paper-based electrochemical cells. The integrated printed paper electrodes, however, showed reduced sensitivities towards $[Ni(dmgH)_2]$ complex detection. The low sensitivity was not unexpected due to a lack of interfacial accumulation and adsorption of the formed metal complexes at the porous cellulose matrix electrode surface. As a result, adequate accumulation and preconcentration of the target metal ions to achieve sensitivities in the

ultra-low µg L^{-1} range was not possible. It can be noted that electrode modification by the ERGO-AuNP nanocomposite improved the detection sensitivity over the unmodified electrode and that lower limits of detection are obtained in the presence of electroplated Hg-films due to amalgam formation with excess [$Ni(dmgH)_2$] complexes even at short analysis times for all electrode surfaces. The reported limits of detection and quantitation, while not ideal, were found to be considerably lower than world health organization (WHO), United States environmental protection agency (US-EPA) and South African drinking water standards maximum contamination limits and showcase that the developed printed paper-based electrochemical system could offer a viable alternative to existing solid electrodes particularly for the determination of metal ions not able to be analysed by anodic stripping voltammetry or whose detection is prone to electrode fouling and may require the use of disposable electrodes.

Table 3: A summary of the previously reported sensors and limits of detection (LOD) for Ni^{2+} detection by stripping voltammetric techniques

Metal Ions	Substrate	Technique	Accumulation Time (s)	Dynamic Linear Range (µg L^{-1})	Detection Limit (µg L^{-1})	Reference
Ni^{2+}	DMG-N-SPE	DPAdSV	120	60 - 500	30	[6]
Ni^{2+}	mpBiF-SPCE	AdCSV	180	1 - 10	0.027	[67]
Co^{2+}				1 - 10	0.094	
Ni^{2+}	RBiABE	DPAdSV	30	0.6 - 41	0.18	[68]
Co^{2+}				0.06 – 4.1	0.018	
Ni^{2+}	PbF-SPE	SWV	60	0.6 – 2.9	0.2	[69]
Co^{2+}				0.6 – 5.9	0.3	
Ni^{2+}	SBVE	SWAdCSV	30	0 - 10	0.6	[5]
Ni^{2+}	DMG-CPE	DPAdSV	120	80 - 600	27	[70]
Ni^{2+}	ERGO-PG-MFE	SWAdCSV	210	2 - 16	0.12	[39]
Ni^{2+} with Co^{2+} and Zn^{2+}	NGr-DMG-GCE	SWAdCSV	120	2 - 20	1.5	[71]
Ni^{2+}	NH_3/NH_4Cl-DMG-PPEC/SPCE	SWAdCSV	90	15 - 120	6.27	[63]
Ni^{2+}	ERGO-AuNP-CC-Ag-PPPE	SWAdCSV	120	50 – 500	32.19	This Work

* DMG/N/SPE – Dimethylglyoxime Nafion Screen Printed Electrode; mpBiF-SPCE - Macroporous Bismuth Film Screen-Printed Carbon Electrode; RBiABE - Renewable Bismuth Bulk Annular Band Electrode; PbF-SPE – Lead Film Screen-Printed Electrode; SBVE – Solid Bismuth Vibrating Electrode; DMG-CPE – Dimethylglyoxime Carbon

Paste Electrode; ERGO-PG-MFE – Electrochemically Reduced Graphene Oxide Pencil-Graphite Mercury Film Electrode; NGr-DMG-GCE – Nafion-Graphene Dimethylglyoxime Glassy Carbon Electrode; NH_3/NH_4Cl-DMG-PPEC/SPCE – Ammonia/Ammonium Chloride Dimethylglyoxime Pre-stored Paper-based Electrochemical Cells with Screen-Printed Carbon Electrode.

4.7. Application to Tap Water Samples of the ERGO-AuNP-CC-Ag-PPPE

Tap water samples, collected in our laboratory and real water samples in the Western Cape region of South Africa were applied to the detection of Ni^{2+} ions using the ERGO-AuNP-CC-Ag-PPE in the presence of chelating agent and electroplated Hg film, where necessary. A standard addition method was utilized to (a) detect the presence of Ni^{2+} contaminants in the water sample and (b) show that the developed sensor could be applied in the new sample matrix (tap and filtered real water). No metal cations were detected within the working potential window in the tap water sample under the developed sensor conditions for either platform used. This may be attributed to trace concentrations present below the sensor limits of detection. Upon spiking tap water samples with 150 µg L^{-1} of Ni^{2+} metal cation yielded good recovery percentages for the individual analysis of the metal ions. The recovery percentages were determined using an extrapolation technique to determine the x-intercept and shown in Table 4. Spike concentrations were chosen to bring the metal ion concentration midway into the dynamic linear range of the sensor. Recoveries of 104, 93 and 95 % were reported for test, tap and real water samples, respectively. The findings show that test samples provided the most accurate detection of Ni^{2+} due to a lack of interferents in the water sample. Intermetallic interferences (copper, zinc and cobalt) as well as inorganic halides and organic surfactants, among others could contribute to an error in accuracy greater than 5 %.

Table 4: Recorded recovery percentages in both test and water samples

Ni^{2+} Sample	Original (µg L^{-1})	Added (µg L^{-1})	Found (µg L^{-1})	Recovery (%)
Test Sample	N/D	150	156.48	104.32 ± 7.68
Tap Water Sample	N/D	150	138.86	92.57 ± 9.32
Real Water Sample	N/D	150	141.92	94.61 ± 6.51

5. Conclusions and Future Work

This work describes a simple inkjet printing process for the production of low-cost and disposable carbon-coated, patterned three-electrode systems based on silver nanoparticles (AgNPs) deposited on the commercial photographic paper substrates. The study showcased, for the first time, the feasibility of physical adsorption processes such as adsorptive stripping voltammetry (AdSV) at paper-based electrodes which were previously thought to be difficult or impossible due the large rough surface area and porosity of the cellulose paper matrix. The fabricated Ag-PPE showed good conductivity in the low ohm range. Furthermore, modification of the CC-Ag-PPE with a gold nanoparticle decorated electrochemical reduced graphene oxide (ERGO-AuNP) composite material in the presence of dimethylglyoxime complexing agent, demonstrated improved sensitivity over the unmodified precursor and provided an accurate and simple quantitative analytical approach towards the detection of Ni^{2+} as a testing standard in drinking and real water samples found in Cape Town, South Africa by adsorptive cathodic stripping voltammetry (AdCSV) well below the WHO, USEPA and South African drinking water standards. When compared with conventional solid carbon electrodes, the printed paper-based sensors were found to not have sensitivities and low limits of detection as good as existing sensing systems at short analysis times due to the inability of the formed $[Ni(dmgH)_2]$ complexes to adequately adsorb onto the printed paper electrode surface during the preconcentration step. The results, however, do suggest that the AdSV technique is possible at low-cost and disposable paper-based electroanalytical devices and provide an exciting avenue for further investigation and application to a wider range of analytes not able to be detected by conventional electrochemical methods. Longer analysis times, further electrode modifications, optimization of the printing procedure and parameters as well as kinetic studies can be performed to further improve the device sensitivity for use in resource limited settings on the African continent.

Data Availability Statement

The authors confirm that the data supporting the findings of this study are available within the article and/or its supplementary material. Raw data were generated at The University of the Western Cape, South Africa and the Council for Scientific and Industrial Research. Derived data supporting the findings of this study are available from the corresponding author on request

.

List of Figures

Figure 7: High resolution scanning electron microscope (HRSEM) images of (a) inkjet-printed AgNP, (b) CC-AgNP, (c) ERGO-CC-AgNP and (d) AuNP-ERGO-CC-AgNP working electrodes on photographic paper at 5 kX magnification.

Figure 8: SW-AdCSVs of 300 µg L^{-1} Ni^{2+} at the ERGO-AuNP-CC-Ag-PPPE in the presence of (a) 0.1 M NH_3/NH_4Cl buffer, (b) 10 mg L^{-1} Hg^{3+}, (c) 2 mM DMG and (d) 2 mM DMG and 10 mg L^{-1} Hg^{3+}. Supporting electrolyte: 0.1 M NH_3/NH_4Cl buffer (pH 9.4). SWV instrumental parameters: E_{acc} = -0.7 V, t_{acc} = 120 s, f = 5 Hz and $Ampl$ = 10 mV.

Figure 9: SWASV and corresponding calibration plot of individual analysis of Ni^{2+} obtained at the ERGO-AuNP-CC-Ag-PPE over 50 – 500 µg L^{-1} range. Supporting electrolyte (0.1 NH_3/NH_4Cl Buffer, pH 9.4), deposition time (90 s), deposition potential (- 0.7 V), rotation speed (1000 rpm), frequency (5 Hz), amplitude (0.01 V).

List of Tables:

Table 1: A summary of the recorded electrical parameters; resistance, resistivity, conductivity and sheet resistance for the Ag ink on photography paper after curing at 120^{o}C for 1 hour.

Table 2: A summary of recorded analytical data for the ERGO-AuNP-CC-Ag-PPE over the 50 – 500 µg L^{-1} range.

Table 3: A summary of the previously reported sensors and limits of detection (LOD) for Ni^{2+} detection by stripping voltammetric techniques

Table 4: Recorded recovery percentages in both test and water samples

Conflict of Interest Statement

The authors declare no conflict of interest.

References

[1] Q. Li, H. Liu, M. Alattar, S. Jiang, J. Han, Y. Ma, and C. Jiang, Sci. Rep., **2015**, 5, 16936. doi:10.1038/srep16936.

[2] M. Jaishankar, T. Tseten, N. Anbalagan, B.B. Mathew, and K.N. Beeregowda, Interdiscip. Toxicol., **2014**, 7. 60–72. doi:10.2478/intox-2014-0009.

[3] K.S. Cameron, V. Buchner, and P.B. Tchounwou, Rev. Environ. Health., **2011**, 26, 81–92.

doi:10.1515/REVEH.2011.012.

[4] R. Jugadi, and A.P. Joshi, Ind. J. Chem., **2003**, 42, 94–96. http://hdl.handle.net/123456789/20502

[5] G.M.S. Alves, J.M.C.S. Magalhães, and H.M.V.M. Soares, Electroanalysis, **2013**, 25, 1247–1255. doi:10.1002/elan.201200643.

[6] A. Ferancová, M.K. Hattuniemi, A.M. Sesay, J.P. Räty, and V.T. Virtanen, J. Hazard. Mater., **2016**, 306, 50–57. doi:http://dx.doi.org/10.1016/j.jhazmat.2015.11.057.

[7] X. Fang, S. Wei, J. Kong, Lab Chip, **2014**, 14, 911–5. doi:10.1039/c3lc51246k.

[8] Z. Nie, C.A. Nijhuis, J. Gong, X. Chen, A. Kumachev, A.W. Martinez, M. Narovlyansky, and G.M. Whitesides, Lab Chip, **2010**, 10, 477–483. doi:10.1039/b917150a.

[9] A.W. Martinez, S.T. Phillips, E. Carrilho, S.W. Thomas, H. Sindi, and G.M. Whitesides, Anal. Chem., **2008**, 80, 3699–3707. doi:10.1021/ac800112r.

[10] W. Dungchai, O. Chailapakul, and C.S. Henry, Anal. Chem., **2009**, 81, 5821–5826. doi:10.1021/ac9007573.

[11] J. Noiphung, T. Songjaroen, W. Dungchai, C.S. Henry, O. Chailapakul, and W. Laiwattanapaisal, Anal. Chim. Acta., **2013**, 788. doi:10.1016/j.aca.2013.06.021.

[12] A. Brett, F. Matysik, and M. Vieira, Electroanalysis, **1997**, 9, 209–12. http://onlinelibrary.wiley.com/doi/10.1002/elan.1140090304/abstract.

[13] H. Li, W. Wang, Q. Lv, G. Xi, H. Bai, and Q. Zhang, J. Electrochem. Comm., **2016**, 68, 104-107. doi:10.1016/j.elecom.2016.05.010.

[14] L.Y. Shiroma, M. Santhiago, A.L. Gobbi, and L.T. Kubota, Anal. Chim. Acta., **2012**, 725, 44–50. doi:10.1016/j.aca.2012.03.011.

[15] W. Dungchai, O. Chailapakul, and C.S. Henry, Analyst, **2011**, 136, 77–82. doi:10.1039/c0an00406e.

[16] S. Cinti, D. Talarico, G. Palleschi, D. Moscone, and F. Arduini, Anal. Chim. Acta, **2016**, 919, 78-84. doi:10.1016/j.aca.2016.03.011.

[17] S. Cinti, and F. Arduini, Biosens. Bioelectron., **2017**, 89, 107–122. doi:10.1016/j.bios.2016.07.005.

[18] N.J. Walch, F. Davis, N. Langford, J.L. Holmes, S.D. Collyer, and S.P.J. Higson, Anal. Chem., **2015**, 87, 9273–9279. doi:10.1021/acs.analchem.5b01829.

[19] J.A. Adkins, and C.S. Henry, Anal. Chim. Acta., **2015**, 891, 247–254. doi:10.1016/j.aca.2015.07.019.

[20] A. Määttänen, U. Vanamo, P. Ihalainen, P. Pulkkinen, H. Tenhu, J. Bobacka, and J. Peltonen, Sensors Actuators, B Chem., **2013**, 177, 153–162. doi:10.1016/j.snb.2012.10.113.

[21] Y.H. Kahng, M.K. Kim, J.H. Lee, Y.J. Kim, N. Kim, D.W. Park, and K. Lee, Sol. Energy Mater. Sol. Cells, **2014**, 124, 86–91. doi:10.1016/j.solmat.2014.01.040.

[22] K. Kim, S. Il Ahn, and K.C. Choi, Carbon N. Y., **2014**, 66, 172–177. doi:10.1016/j.carbon.2013.08.055.

[23] F. Molina-Lopez, D. Briand, and N.F. De Rooij, Sensors Actuators, B Chem., **2012**, 166, 212–222. doi:10.1016/j.snb.2012.02.042.

[24] T. Öhlund, J. Örtegren, S. Forsberg, and H.E. Nilsson, Appl. Surf. Sci. **2012**, 259, 731–739. doi:10.1016/j.apsusc.2012.07.112.

[25] T. Hibbard, K. Crowley, and A.J. Killard, Anal. Chim. Acta., **2013**, 779, 56–63. doi:10.1016/j.aca.2013.03.051.

[26] N. Dossi, R. Toniolo, A. Pizzariello, F. Impellizzieri, E. Piccin, and G. Bontempelli, Electrophoresis, **2013**, 34, 2085–2091. doi:10.1002/elps.201200425.

[27] K. Abe, K. Suzuki, and D. Citterio, Anal. Chem., **2008**, 80, 6928–6934. doi:10.1021/ac800604v.

[28] A. Moya, G. Gabriel, R. Villa, F. Javier del Campo, Curr. Opin. Electrochem., **2017**, 3, 29–39. doi:10.1016/j.coelec.2017.05.003.

[29] R. Tortorich, H. Shamkhalichenar, and J.-W. Choi, Appl. Sci., **2018**, 8, 288–304. doi:10.3390/app8020288.

[30] P. Sjöberg, A. Määttänen, U. Vanamo, M. Novell, P. Ihalainen, F.J. Andrade, J. Bobacka, and J. Peltonen, Sensors Actuators, B Chem., **2016**, 224, 325–332. doi:10.1016/j.snb.2015.10.051.

[31] A. Romeo, A. Moya, T.S. Leung, G. Gabriel, R. Villa, and S. Sánchez, Appl. Mater. Today, **2018**, 10, 133–141. doi:10.1016/j.apmt.2017.12.016.

[32] E. Song, R.P. Tortorich, T.H. Da Costa, and J.W. Choi, Microelectron. Eng., **2015**, 145, 143–148. doi:10.1016/j.mee.2015.04.004.

[33] Y. Qin, H.J. Kwon, A. Subrahmanyam, M.M.R. Howlader, P.R. Selvaganapathy, A. Adronov, and M.J. Deen, Mater. Lett., **2016**, 176, 68–70. doi:10.1016/j.matlet.2016.04.048.

[34] A. Moya, E. Sowade, F.J. del Campo, K.Y. Mitra, E. Ramon, R. Villa, R.R. Baumann, and G. Gabriel, Org. Electron. Physics, Mater. Appl., **2016**, 39, 168–176. doi:10.1016/j.orgel.2016.10.002.

[35] W. Kit-Anan, A. Olarnwanich, C. Sriprachuabwong, C. Karuwan, A. Tuantranont, A. Wisitsoraat, W. Srituravanich, and A. Pimpin, J. Electroanal. Chem., **2012**, 685, 72–78. doi:10.1016/j.jelechem.2012.08.039.

[36] G. Herzog, V. Beni, Anal. Chim. Acta, **2013**, 769, 10–21. doi:10.1016/j.aca.2012.12.031.

[37] K. Pokpas, S. Zbeda, N. Jahed, N. Mohamed, P.G. Baker, and E.I. Iwuoha, Int. J. Electrochem. Sci., **2014**, 9, 736–759. www.electrochemsci.org.

[38] K. Pokpas, N. Jahed, O. Tovide, P.G. Baker, E.I. Iwuoha, Int. J. Electrochem. Sci., **2014**, 9, 5092–5115. www.electrochemsci.org.

[39] R. Tekenya, K. Pokpas, N. Jahed, and E.I. Iwuoha, Anal. Lett., **2018**, 0, 1–26. doi:10.1080/00032719.2018.1469139.

[40] S.A. Kitte, S. Li, A. Nsabimana, W. Gao, J. Lai, Z. Liu, G. Xu, Talanta. **2019**, 191, 485–490. doi:10.1016/j.talanta.2018.08.066.

[41] C. Kokkinos, A. Economou, Sensors Actuators B Chem. **2016**, 229, 362–369. doi:10.1016/j.snb.2016.01.148.

[42] C. Rojas-Romo, N. Serrano, C. Ariño, V. Arancibia, J.M. Díaz-Cruz, M. Esteban, Talanta. **2016**, 155, 21–27. doi:10.1016/j.talanta.2016.04.015.

[43] X. Yiwei, L. Zhihua, Z. Wen, S. Jiyong, Z. Xiaobo, H. Xiaowei, H. Xuetao, W. Xin, Anal. Lett. **2019**, 52, 2938–2950. doi:10.1080/00032719.2019.1631839.

[44] R. Segura, M. Pradena, D. Pinto, F. Godoy, E. Nagles, V. Arancibia, Talanta. **2011**,85, 2316–2319. doi:10.1016/j.talanta.2011.07.062.

[45] A. Bobrowski, A. Królicka, Insights in Anal. Chem., **2015**, 1, 1–6. doi:10.21767/2470-9867.100006.

[46] A. Bobrowski, A. Krolicka, M. Maczuga, J. Zarebski, Electroanalysis. **2016**, 28, 343–349. doi:10.1002/elan.201500362.

[47] S. Wu, X. Huang, Y. Wu, L. Luo, Y. Jin, Q. Li, Int. J. Electrochem. Sci. **2015**, 10, 8255–8262. www.electrochemsci.org (accessed April 3, 2017).

[48] B. Silwana, C. van der Horst, E. Iwuoha, V. Somerset, Electroanalysis. **2016**, 28, 1597–1607. doi:10.1002/elan.201501071.

[49] X. Yiwei, Z. Wen, H. Xiaowei, S. Jiyong, Z. Xiaobo, L. Yanxiao, C. Xueping, H.E. Tahir, L. Zhihua, Electroanalysis. **2018**, 30, 194–203. doi:10.1002/elan.201700637.

[50] Y. Xu, W. Zhang, X. Huang, J. Shi, X. Zou, Z. Li, X. Cui, **2019**, Microchem. J. 149, 104022. doi:10.1016/j.microc.2019.104022.

[51] F.F. Hudari, J.C. Souza, and M.V.B. Zanoni, Talanta, **2018**, 179, 652–657. doi:10.1016/j.talanta.2017.11.071.

[52] B. Karbowska, and R. Tomasz, Int. J. Environ. Res. Public Health, **2018**, 15, 653. doi:10.3390/ijerph15040653.

[53] A. Simpson, R.R. Pandey, C.C. Chusuei, K. Ghosh, R. Patel, and A.K. Wanekaya, Carbon N. Y., **2018**, 127, 122–130. doi:10.1016/j.carbon.2017.10.086.

[54] R. Liu, Y.J. Tan, T. Zhong, and C. Lei, Anal. Lett., **2018**, 51, 2351–2361. doi:10.1080/00032719.2018.1424174.

[55] A. Wong, A.M. Santos, and O. Fatibello-Filho, Sensors Actuators, B Chem., **2018**, 255 (2018) 2264–2273. doi:10.1016/j.snb.2017.09.020.

[56] L. Li, D. Liu, A. Shi, and T. You, Sensors Actuators, B Chem., **2018**, 255, 1762–1770. doi:10.1016/j.snb.2017.08.190.

[57] G.M. Durán, E.J. Llorent-Martínez, A.M. Contento, and Á. Ríos, Microchim. Acta., **2018**, 185, 1–8. doi:10.1007/s00604-018-2738-1.

[58] C.M.A. Brett, M.B.Q. Garcia, and J.L.F.C. Lima, Electroanalysis, **1996**, 8, 1169–1173. doi:10.1002/elan.1140081219.

[59] J. William S. Hummers, and R.E. Offeman, J. Am. Chem. Soc., **1958**, 80 (1958) 1339. doi:10.1021/ja01539a017.

[60] T.H. Joubert, P.H. Bezuidenhout, H. Chen, S. Smith, and K.J. Land, Mater. Today Proc., **2015**, 2, 3891–3900. doi:10.1016/j.matpr.2015.08.018.

[61] B. Wu, N. Zhao, S. Hou, and C. Zhang, Nanomaterials., **2016**, 6, 220. doi:10.3390/nano6110220.

[62] L. Baxter, A. Bobrowski, M. Bond, G. Heath, R.L. Paul, R. Mrzljak, J. Zarebski, Anal. Chem., **1998**, 70, 1312–23. doi:10.1021/ac9703616.

[63] K. Pokpas, N. Jahed, and E.I. Iwuoha, Electrocatalysis, **2019**, 10, 352-364. doi: 10.1007/s12678-019-00516-7

[64] D.D. Liana, B. Raguse, J. Justin Gooding, E. Chow, J.J. Gooding, E. Chow, Sensors, **2012**, 12, 11505–11526. doi:10.3390/s120911505.

[65] E.J. Maxwell, A.D. Mazzeo, G.M. Whitesides, MRS Bull. **2013**,38, 309–314. doi:10.1557/mrs.2013.56.

[66] Y. Ko, M. Kwon, W.K. Bae, B. Lee, S.W. Lee, J. Cho, Nat. Commun. **2017**, 8, 1–10. doi:10.1038/s41467-017-00550-3.

[67] S. Dal Borgo, H. Sopha, S. Smarzewska, S.B. Hočevar, I. Švancara, and R. Metelka, Electroanalysis, **2015**, 27 , 209–216. doi:10.1002/elan.201400422.

[68] B. Bas, K. Wegiel, and K. Jedlinska, Anal. Chim. Acta., **2015**, 881, 44–53. doi:10.1016/j.aca.2015.05.005.

[69] A. Bobrowski, A. Królicka, M. Maczuga, and J. Zarębski, Sensors Actuators, B Chem., **2014**, 191, 291–297. doi:10.1016/j.snb.2013.10.006.

[70] A. Ferancová, M.K. Hattuniemi, A.M. Sesay, J.P. Räty, and V.T. Virtanen, Mine Water Environ., **2015**, 35, 547–552. doi:10.1007/s10230-015-0357-1.

[71] K. Pokpas, N. Jahed, P.G. Baker, and E.I. Iwuoha, Sensors, **2017**, 17, 1711. doi:10.3390/S17081711.